Intracellular molecular diffusion probed with nonlinear optical microscopy

Potma, Eric Olaf

Chapter 2

Cavity-dumped optical parametric oscillator

A multicolor femtosecond light source for nonlinear optical microscopy

Abstract

In this chapter we present a tunable femtosecond light source that is ideally suited for nonlinear microscopy. The system consists of a visible optical parametric oscillator (OPO) that is pumped by the second harmonic of a Ti:sapphire laser. The OPO delivers 30-fs pulses tunable between 570 to 660 nm with energies as high as 13 nJ. A cavity-dumper inserted into one of the arms of the resonator provides a means to vary the pulse repetition rate over a frequency range up to 4 MHz. The time-jitter between the pulses of the Ti:sapphire pump laser and the cavity-dumped OPO is smaller than 30-fs, permitting multicolor time-resolved spectroscopic experiments. Its tunable multicolor output and the option to balance pulse peak powers against the average illumination dose make the system a consummate light source for nonlinear microscopy investigations of biological objects.

Parts of this chapter can also be found in the following papers:

E. O. Potma, W. P. de Boeij, M. S. Pshenichnikov and D. A. Wiersma, "A 30-fs, cavity-dumped optical parametric oscillator", *Opt. Lett.* **23**, 1763-1765 (1998).

E. O. Potma, N. Kahya, W. P. de Boeij and D. A. Wiersma, "A multicolor femtosecond light source for (multiphoton) confocal fluorescence microscopy", *Microscopy and Microanalysis* **5 (Suppl. 2)**, 472-473 (1999).

2.1 Introduction

Triggered by the first demonstration of microscopic multiphoton excitation in biological samples [1], the fruitful amalgamation of nonlinear spectroscopy and optical microscopy was soon recognized. Exploitation of nonlinear interactions in confined focal volumes has provided new ways of probing cellular specimens and has intensified the significance of optical techniques as indispensable tools in biological research. Next to multiphoton excitation of fluorophores, coherent nonlinear methods such as second- and third harmonic generation and coherent anti-Stokes Raman scattering have been successfully applied in a microscope configuration [1-4]. Besides their specific spectroscopic sensitivity, all these methods offer the microscopist inbuilt advantages like inherent optical sectioning, reduced out-of-focus bleaching and higher penetration depths into the sample.

A profitable implementation of nonlinear techniques in an optical microscope puts some demands on the light source employed. To promote the nonlinear response at the focal point, appreciable excitation intensities are required. At the same time, to avert photoinduced damage, the illumination dose applied to the sample should not be excessively high. The use of a subpicosecond pulsed light source meets these requirements as it provides high peak powers while keeping the average power at benign levels [5,6]. For the routine application of nonlinear optical microscopy in the biologist's laboratory, the laser system ought furthermore to be robust, exhibit excellent stability and pulse characteristics, and should ideally be tunable over a broad spectral range. In this regard, the commercial availability of reliable solid-state pulsed light sources like the Ti:sapphire laser, has been the underpinning for the wealth of nonlinear microscopic studies reported in literature nowadays [7-10].

Despite the impressive tuning range of the commonly used Ti:sapphire laser output (700 – 1000 nm) in conjunction with its second harmonic (350-500 nm), a broad inaccessible gap is left in the visible spectral regime. Thus, a large span of fluorophores that absorb in the 250-350 nm window, fall outside the two-photon addressable reach of the Ti:sapphire laser. This implies that a number of biologically relevant fluorophores like tryptophan and tyrosine cannot be addressed in a two-photon process [11]. Similarly, several widely used fluorescent labels like cascade blue, coumarin and naphtalene derivatives as well as caged bioprobes absorb within this energy range. For these reasons, a light source exhibiting operational characteristics similar to the Ti:sapphire laser but with a tunability range that includes the visible spectral region would be highly beneficial.

Parametric down-conversion techniques offer a convenient means to generate optical frequencies beyond the emission spectra of conventional laser systems. In the nonlinear parametric process a high-energy photon is converted into two photons of lower energies. Shortly after the invention of the laser, the nonlinear process of parametric frequency conversion was demonstrated and its potential as a coherent source of radiation was established accordingly [12-17]. Over the years, the availability of new pump sources and nonlinear materials, next to a better grasp of the optimum configuration of the interacting beams, has given rise to extremely efficient frequency conversion schemes [18-25]. This has led to parametric generation of light over a virtually unlimited spectral range that stretches from the UV to the far-infrared,

encompassing ultrashort femtosecond pulses to continuous-wave coherent radiation at almost any desirable power level [26-32]. In the visible regime, for reasons of robustness and flexibility, parametric frequency conversion methods have at present largely replaced conventional dye-laser systems.

To generate appreciable levels of visible pulsed radiation parametrically, two common routes exist to overcome to low efficiency of the parametric process. One of these schemes comprises the optical parametric amplification of visible wavelengths in a nonlinear medium pumped by the intense second harmonic radiation of a mode-locked Ti:sapphire laser. Exploiting the remarkably extensive parametric bandwidth of β-barium borate (BBO), this strategy has been demonstrated to enable the generation of pulses exhibiting an outstandingly broad spectral width [33-37]. Using appropriate pulse compression techniques, pulses with temporal widths down to 6 fs have been achieved in this way [35,38-40]. However, this scheme is connected to an involved regenerative Ti:sapphire amplification chain. Moreover, the high pulse energies (up to 10 μJ) delivered by the optical parametric amplifier (OPA) system are much too high for optical microscopy. Additionally, the reduced repetition rate of these systems amounts to typically one- or several kHz and are thus incompatible with the fast pixel integration times needed in the imaging process.

A second approach is to synchronously pump an optical parametric oscillator (OPO). With typical pulse powers in the nJ range and a less complex experimental layout, the utilization of parametric oscillators constitutes a route that shows more overlap with the requisites associated with nonlinear microscopy in a routine laboratory. Following this route, generation of visible femtosecond radiation has been accomplished by subsequent frequency up-conversion of the radiation of near-infrared OPO's, either intra- or extra-cavity [41-43]. An alternative method is the direct parametric generation of visible light using BBO as the nonlinear medium. This latter approach in particular offers many advantages like tunability and system robustness. As was recently shown by Driscoll et al. [44,45], a BBO-based OPO pumped with the frequency-doubled output of a Ti:sapphire laser permits the generation of ultrashort pulses within a tuning range from 565 nm to 675 nm at 1.5 nJ pulse powers. If interfaced with an optical microscope, such a system would provide a versatile all-solid-state solution that fills the breach in the visible regime left by the conventional Ti:sapphire-based laser systems.

The synchronous pumping mechanism of the OPO inherently entails parametric signal outputs with repetition rates in the 100 MHz range. The limited time span between the individual pulses raises a number of experimental complications. For instance, to maintain noticeable peak powers needed to assess the nonlinear process, the average power may reach a level harmful to living cells. In this sense, reducing the number of pulses applied to the sample per time unit, thereby lowering the average illumination dose, would be advantageous. Another problem related to the high repetition rate is encountered in fluorescence lifetime imaging experiments. With typical fluorescence lifetimes in the nanosecond range, once excited with a short laserpulse, the excited population may have incompletely relaxed to the ground state when the next pulse arrives. This leads to unwanted accumulation effects that hamper an accurate lifetime determination [46]. Similarly, in many time-resolved (micro-)spectroscopic measure-ments a high repetition rate may seriously interfere with ongoing dynamics of

the excited molecular species. Again, an increase of the inter-pulse separation would ameliorate the reliability of the experiment considerably.

To vary the repetition rate of the light source, the technique of cavity-dumping has been successfully employed in mode-locked dye lasers and solid state lasers alike [47-51]. In this way, dumped pulses as short as 13 fs have been achieved with 60 nJ peak energies at repetition rates up to 200 kHz [49]. Besides a favorable increase of the pulse energy, it was furthermore shown that incorporation of a cavity-dumper in the resonator essentially preserves the operational characteristics of the laser system. The question arises whether a similar technique can be utilized to adjust the repetition frequency of a synchronously-pumped optical parametric oscillator.

In this chapter we show that a visible parametric oscillator can be efficiently cavity-dumped, boosting the output pulse's energy by a factor of 10 [52]. It is furthermore demonstrated that the excellent output properties of the BBO-based oscillator are maintained with the dumper inserted. The system is capable in delivering 30 fs pulses with energies as high as 13-nJ at repetition rates up to 400 kHz. The broad tuning range extends from 570 to 670 nm. Equipped with the cavity-dumper, the visible OPO is a flexible light source for nonlinear optical microscopy.

The organization of this chapter is as follows: In section 2.2 the principles of parametric light generation are outlined. Also, a cavity design of the visible OPO is presented that exploits the favorable parametric interaction in BBO. Next, in section 2.3, the operation of the OPO with a cavity-dumper incorporated into the resonator is discussed. A detailed account on the intracavity dispersion and its subsequent influence on the duration of the pulses can also be found in this section. The multicolor capability of the system is dealt with in section 2.4 and its applications in optical microscopy and molecular spectroscopy are pointed out. Finally, in section 2.5, we summarize our findings and provide some concluding remarks.

2.2 Visible femtosecond optical parametric light generation

In this section the fundamentals of parametric amplification are addressed. Some factors that influence the efficiency of the parametric process are introduced to the reader. In particular, the concept and implications of noncollinear phase-matching in BBO are considered. We show how the virtues of the nonlinear parametric process are exemplified in the practical realization of a resonator system. Connected to this, the main operating characteristics of the parametric oscillator are discussed.

2.2.1 Principles of optical parametric amplification

The nonlinear optical phenomenon of parametric light generation was first treated theoretically in 1962 [12]. In the parametric process, a pump wave with energy ω_p is converted into a signal and an idler wave that oscillate at frequency ω_s and ω_i respectively. Since energy is conserved in this process, the parametric effect comprises the downconversion of a high-energy photon into two lower-energy photons:

$$\omega_p = \omega_s + \omega_i \tag{2.1}$$

Accordingly, the parametric effect may result in any combination of signal and idler frequencies, as long as the requirement of energy conservation is met. Here the initial parametric waves are either build up from the optical quantum noise or are seeded with light from a second source. Hence, as opposed to laser devices, the parametric process constitutes a means of light generation that is not bound to specific optical transitions. However, several mechanisms limit the boundless generation of optical frequencies. Since parametric amplification proceeds in a coherent manner, signal and idler waves only accumulate constructively if the phases of the waves involved are appropriately matched. A criterion that needs to be fulfilled is the condition of conservation of momentum:

$$\boldsymbol{k}_p = \boldsymbol{k}_s + \boldsymbol{k}_i \tag{2.2}$$

where $\boldsymbol{k}$ designates the wave vector. Because the wave vectors scale with the refractive index of the medium, efficient parametric light generation only occurs under specific circumstances, in which condition (2.2) is satisfied. Such a situation is for instance encountered in birefringent materials using a specific phase matching geometry.

We restrict our discussion to uniaxial crystals, which are birefringent materials characterized by a single optic axis. In this case, phase-matching can be accomplished in various ways [53]. Type I phase matching applies when the polarization of both the signal and idler waves are orthogonally oriented with respect to the pump polarization. Alternatively, if the signal and idler are perpendicularly polarized relative to each other, the phase-matching scheme is classified as Type II. The polarization of the light beams is defined by the its direction with respect to the principal plane of the crystal that contains the wave vector $\boldsymbol{k}$ and the optic axis of the crystal. When normal to the principal plane, the polarization direction is called “ordinary” (o). The polarization direction parallel to the principal plane is known as “extraordinary” (e). In actualizing each of the polarization permutations (Eq. (2.2)), the phase-matching criterion is fulfilled for a specific phase-matching angle θ_{pm} as defined by the angle between the incident wave vector and the optic axis. Following this reasoning, only single signal and idler frequencies appear for a particular realization of the phase-matching condition. Practically this implies that wavelength tuning of the parametric signal requires a corresponding adaptation of the phase-matching geometry, which is for instance realized when reorienting the crystal.

Besides the nonlinearity $d_{eff}^{(2)}$ of the crystal and the phase-matching criterion, the efficiency of the parametric conversion process is influenced by a phenomenon that is known as beam “walk-off”. In uniaxial crystals, the direction of propagation of the wave vector of an extraordinary beam does not coincide with its flow of wave energy as given by the Poynting vector $\boldsymbol{S}$. The angle between $\boldsymbol{k}$ and $\boldsymbol{S}$ is called the spatial walk-off angle ρ[53]. A large walk-off angle will deplete the pump energy along the phase-matched direction, thereby affecting the efficacy of the frequency conversion process [54].

When ultrashort pulsed radiation is employed, the details of the parametric generation mechanism are furthermore shaped by the temporal evolution of the light pulses involved. Because of the dispersion properties of the medium, the propagation velocity of light is dependent on the optical frequency. Conditional on the crystal length and the duration of the pulses, the difference in group velocity introduces a temporal

mismatch among the interacting waveforms. This phenomenon is also noted as group velocity mismatch. For sub-100 fs pumping radiation in the visible regime the group velocity mismatch already starts to affect the conversion efficiency considerably in a typical nonlinear material with a thickness of 1 mm. In addition to this, higher order dispersion effects also deteriorate the efficiency of the parametric process. In particular, group delay dispersion (GDD) establishes a temporal broadening of the light pulses in the normal dispersion regime, resulting in a temporal chirp of frequency components within the pulse. Notably for short pulses that encompass broad spectra, the induced chirp enforces complicated variations in the temporal overlap of the frequency components of the pump, signal and idler beams [55-57].

Clearly, for a sophisticated description of the parametric process, all the above mentioned effects should be taken into the consideration. To account for these and other limiting mechanisms such as pump depletion and cascaded nonlinear processes, analytical solutions can not be given and numerical schemes are required to evaluate the resulting signal and idler fields [55,57,58].

When the parametric process is utilized as a gain source in a cavity configuration, multiple passes through the nonlinear medium awaken the progressive amplification of the parametric light. Given the optical losses of the resonator, an intra-cavity coherent signal may build up to appreciable steady-state powers. Optical parametric oscillation is based on this condition which occurs when the parametric gain overcomes the total cavity losses [16].

2.2.2 Noncollinear parametric generation in β-barium borate

The discussion above emphasizes that optimization of the parametric process incorporates a careful consideration of relevant parameters such as effective nonlinearity, phase-matching geometry and dispersive properties of the material. In this sense, the choice of a particular crystal is a decisive factor. For our particular application BBO is utilized as the nonlinear medium to generate a parametric signal in the visible spectral range. The BBO crystal is a uniaxial birefringent material that exhibits excellent properties for the optimization of the parametric process. Next to a high nonlinear susceptibility ($d_{eff}^{(2)} \sim$ 2 pm/V) the crystal is characterized by a broad transparency range that spans from 190 nm up to 3 μm. Furthermore, the damage threshold of BBO is among the highest known for nonlinear crystals [53,59].

Next to these beneficial material properties, BBO is renowned for its exceptionally broad spectral parametric bandwidth when pumped with 400-nm radiation. As demonstrated by Driscoll et al. [44], a specific noncollinear phase-matching arrangement exists that promotes parametric generation throughout practically the entire visible spectral range. In this configuration the wave vector of the pump makes an inclination angle of 3.7º with the propagation direction of the signal beam. Type I phase-matching is enforced, in which signal and idler have ordinary polarization and the pump beam is polarized with an extraordinary orientation. Compared to Type II phase-matching, the present geometry is accompanied with a higher nonlinear response of the BBO crystal. Moreover, the parametric bandwidth is much broader in case of Type I.

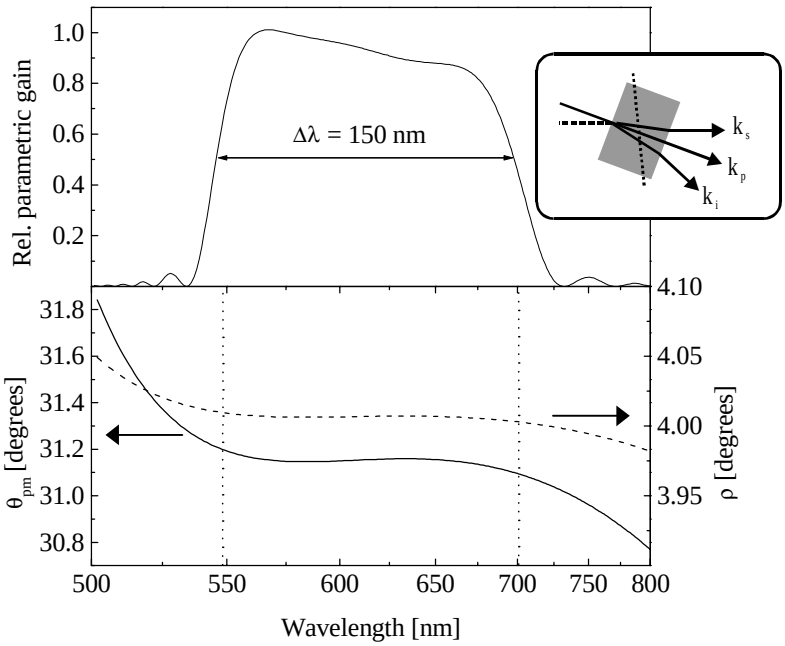

Figure 2.1. Parametric generation of visible light in β-barium borate under a noncollinear phasematching geometry. Upper panel shows the calculated parametric bandwidth in the limit of low-level signal gain, using a 1.5-mm BBO crystal pumped by 400 nm and adopting an angle of 3.7 degrees between the pump and signal directional wavevectors. The optimum bandwidth is obtained for a phasematching angle θ_{pm} = 31.2°. The corresponding phase matching geometry is sketched in the inset, with the crystal axis (dotted line) and signal propagation direction (dashed line) indicated. As is indicated by the solid line in the lower panel, θ_{pm} is almost invariant throughout the visible range (marked by dotted vertical lines). Additionally, the walk-off angle of ρ = 4º is virtually constant in this spectral region (dashed line).

Figure 2.1 depicts the corresponding variation of the phase-matching angle as a function of the wavelength of the parametric signal. It can be seen that for a phase-matching angle θ_{pm} of 31.2 degrees parametric generation becomes extremely tolerant to the signal wavelength. When such an angle is adopted, a theoretical calculation shows that the parametric gain extends over 150 nm. Hence, a single geometrical setting of the crystal suffices for the generation of a broad parametric emission spectrum. This recommended phase-matching configuration is thus highly conducive for ultrashort pulse generation.

The noncollinear beam geometry exerts furthermore a favorable influence on the efficiency of the parametric process [60,61]. By coincidence, the spatial walk-off angle of the extraordinary pump beam measures 4.0º, which is close to the 3.7º inclination angle between the pump and the propagation direction of the signal waves. This implies that the pathlength of spatial overlap of the signal and pump in the crystal is significantly enhanced with respect to a collinear alignment of the interacting beams.

As is displayed in Figure 2.1, the walk-off angle is almost invariant over the parametric bandwidth, ensuring advantageous walk-off compensation for all generated signal frequencies. Yet another fortuitous compensation scheme arises from the diminished group velocity mismatch in the noncollinear geometry. In the noncollinear arrangement both the signal and idler, which are red-shifted relative to the pump, cover a longer pathlength in the medium than the pump beam. The longer travel distances of the parametric beams counterbalance to a certain extent the higher group velocities involved. As a result, temporal overlap during interaction is fairly optimized which adds to improved amplification of the parametric signal contributions [60].

2.2.3 BBO-based visible optical parametric oscillator

The layout of the visible femtosecond OPO system is given in Figure 2.2. The design of the OPO mainly follows the one previously described in Ref. [44]. A 12.5 W large-frame argon ion laser is used to pump a Ti:sapphire laser that produces 2.0 W, 50-fs pulses with central wavelength of 800 nm at a 82 MHz repetition rate.

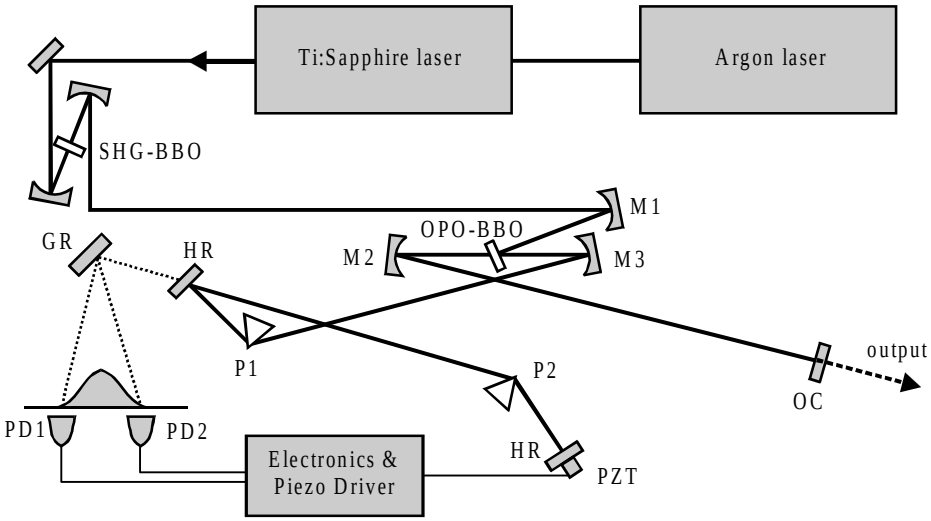

Figure 2.2. Layout of visible fs OPO. Argon laser: Spectra Physics model 2080; Ti:sapphire laser: Spectra Physics Tsunami; SHG-BBO: second-harmonic BBO crystal (thickness 2-mm, cut angle φ =29°, Castech); OPO-BBO: 1.5 thick BBO crystal (φ=31°, Castech); M1: pump focusing mirror (radius of curvature r = -125 mm, CVI); M2,M3: intracavity focusing mirrors (r = -100 mm, CVI); HR: high reflector mirror; OC: 3% output coupler (CVI); PZT: piezo transducer (Physik Instrumente); P1-P2: Brewster-angle fused silica prisms; GR: diffraction grating. PD1,PD2: photodiodes. Note that in reality the pump and intracavity beams are displaced in the vertical plane.

The output of the Ti:sapphire laser is frequency-doubled in a 2-mm BBO crystal with more than 50% power efficiency. As a result of spectral narrowing, dispersion and spatial beam walk-off, the resulting 400 nm pulses exhibit a temporal width of 140 fs. The blue pulses are focused with a curved mirror in a 1.5-mm BBO crystal cut at 31.2º for noncollinear phase-matching. The distance between the SHG crystal and the parametric medium measures 47 cm.

The BBO-based parametric oscillator is singly resonant as it is aimed to amplify the visible parametric signal while the associated idler wave is not matched with a cavity mode. A linear cavity configuration is adopted. The nonlinear crystal is placed at the location of the shared focal spot of two parfocally positioned curved mirrors. The orientation of the mirrors is chosen such as to compensate for astigmatism introduced by the BBO crystal. Pump induced parametric fluorescence is collimated by the curved mirror (M2) and forwarded into one of the cavity arms. This arm contains a fused silica prism pair to compensate for intracavity group delay dispersion. The prism apex-to-apex spacing is 61 cm. A high reflective folding mirror is positioned in the optical path in between the prisms to make the oscillator more compact. On travelling in opposite direction, the parametric signal pass the crystal for a second time. No amplification of the signal occurs on traversing the crystal, due to absence of a pump pulse at this time. Next, the pulses enter the other arm of the resonator that includes a 3% output coupler. In a subsequent pass through the nonlinear crystal, the parametric pulse meets the following pump pulse and signal amplification follows. To ensure intensification of the parametric signal at every complete roundtrip, the temporal overlap of the pump and signal pulses at the position of the BBO crystal requires the total cavity round trip time to match the repetition rate of the pumping radiation.

With the resonator aligned properly, lasing occurs for pump powers as low as 520 mW. The pump depletion amounts up to 45%. The lowest order transverse mode profile is smooth and does not exhibit prominent side-lobes. Higher-order transverse mode patterns up to the sixth order (TEM_{06}) are clearly observed when deliberately misaligning the oscillator [62].

Although the noncollinear beam geometry supports a large parametric bandwidth, not every signal wavelength is equally amplified in the resonator. Because of intracavity dispersion, each signal color will acquire a distinct roundtrip time. Consequently, only those wavelengths that fall within a tolerable spectral range experience sufficient temporal overlap with the pump to raise the level of parametric gain above the optical losses. As a result, the spectral width of the signal is much smaller than the theoretical parametric spectrum. Therefore, the potential application of the visible OPO to generate ultrashort pulses is connected to means to control the intracavity dispersion. A more detailed analysis of the dispersion properties of the parametric oscillator and its effect on pulse duration will be presented in the next section.

A box encloses the parametric oscillator to minimize the obtrusive influence of air flow and dust deposition. Still, the synchronously pumped OPO is fairly sensitive to small variations in the repetition frequency of the Ti:sapphire master oscillator, which irrevocably introduce a temporal jittering of the amplification process. In order to eliminate frequency fluctuations, the repetition rate of the Ti:sapphire laser is locked to an external reference oscillator. The scheme includes a feedback loop that controls a

piezo transducer attached to one of the intracavity mirrors of the Ti:sapphire resonator [63].

Any low frequency acoustic and thermal length variations of the OPO cavity will also introduce temporal and wavelength dependent fluctuations in the signal output. To overcome this problem, the OPO pulse spectrum is actively stabilized. A grating disperses the signal that leaks through a high reflective mirror and projects the pulse spectrum onto two photodiodes. The differential signal of the photodiodes is subsequently used to drive a piezo transducer that controls the position of the cavity end mirror [64]. Any variation of the central wavelength will be translated in an adjustment of the cavity length. This scheme appoints the central wavelength to a fixed position with a high stability on a timescale ranging from 10 ms to several hours. In particular, spectral stabilization appears to be crucial in maintaining broad pulse spectra, as explained in the next section. Another source of power instability traces back to the argon pump laser. Given the consecutive frequency conversions of the Ti:sapphire laser and the SHG that precede the parametric process, original noise of the argon laser is significantly enhanced at the stage of the OPO. Therefore, the performance of the OPO benefits enormously from an intensity stabilized circuit (Silent Light, Spectra Physics) of the argon pump laser, reducing low (dc–sub–kHz) frequency noise. With these feedback circuits the fluctuations of the intracavity pulse power do not exceed 5%. As such, the day-to-day OPO operation usually requires only a slight cavity length adjustment, after the pump lasers have warmed up.

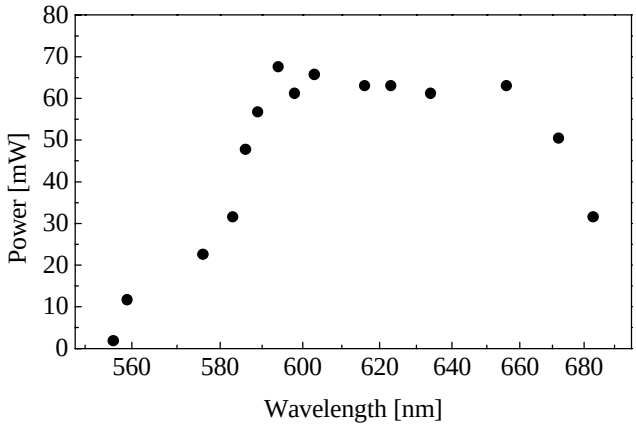

Figure 2.3. Tunable output power of the synchronously-pumped visible femtosecond OPO. The linear OPO cavity incorporates a 1.5-mm BBO crystal and a 3% output coupler. The total tunable range spans more than 120 nm.

The large parametric bandwidth allows tuning of the central wavelength of the signal over an extended range. Figure 2.3 shows the output power of the OPO as a function of the signal wavelength for the linear cavity design. Tuning is realized by adjusting the cavity length and prism setting. The tunable range extends from 556 to 681 nm and output powers as high as 65 mW are obtained. The tunability of the OPO falls well

within the parametric bandwidth of the crystal. Due to wavelength dependent cavity losses that manifest themselves predominantly at the high and low energy side of the gain spectrum, the resultant tunability is yet somewhat smaller than the parametric bandwidth. Note that in case the 1.5-mm thick parametric crystal is substituted with a 2.0-mm BBO crystal, signal powers up to 75 mW are obtained utilizing a 3% output coupler. These numbers compare with the power levels of a similar OPO system reported in Ref [44]. However, due to detrimental reflective properties of the thicker crystal, we find that the tunability range is rather limited.

When the linear resonator is reconfigured into a folded-six-mirror ring cavity, the intracavity power level is significantly enhanced. In a ring-like synchronously-pumped parametric oscillator, the signal traverses the cavity uni-directionally and undergoes pump-induced amplification at every passage through the crystal. The reflective round-trip losses experienced by the signal pulse are reduced accordingly. For this reason, output powers exceeding 120 mW are achieved and the spectral tuning range is somewhat broader. Also, the ring resonator supports broader pulse spectra. In case the generation of ultrashort pulses is the primary goal, the ring design of the oscillator is preferable over the linear cavity [45].

2.3 Cavity-dumped OPO

In this section cavity dumping of the visible optical parametric oscillator is demonstrated. The configuration of the cavity-dumped resonator is motivated and the operational details are presented. Specifically, the role of intracavity dispersion is emphasized. It is shown that short femtosecond cavity-dumped pulses can be obtained over the entire tunable range of the OPO.

2.3.1 Cavity dumping of the parametric oscillator

The repetition rate of the OPO signal is dictated by the Ti:sapphire master oscillator, which is fixed at 82 MHz. Many optical experiments require however lower repetition frequencies to reduce either the average excitation power applied to the sample or to avoid unwanted accumulation effects. Two possible schemes can be applied to lower the repetition rate of the parametric signal pulses without affecting the operating characteristics of the OPO dramatically. The first approach consists of extra-cavity pulse-picking of the signal beam. Given the maximum output power of the linear OPO, a corresponding pulse energy of 0.8 nJ would result for a 100% pulse extraction efficiency. In practice however, this efficiency will be considerably lower. Since the success of many nonlinear optical applications relies on pulse intensity, insufficient energy may be delivered when using the extra-cavity scheme. The nonlinear experiments described in this thesis for instance, typically require 5 nJ of pulse energy directly from the light source. Extra-cavity parametric amplification at a lower repetition rate is a possible route to overcome this problem. However, this approach involves the availability of intense pump pulses at a low repetition frequency, which naturally implies the participation of a complicated amplification scheme.

An alternative method is based on intra-cavity pulse selection. Since energy is extracted directly from the power stored in the high-Q-cavity, this approach generally leads to higher dumped pulse powers. For this reason, it is this scheme that we will exploit to acquire a lower repetition rate of the OPO. In this study the cavity-dumping is realized with an acoustic-optical modulator. Here, a fused-silica Bragg cell serves to refract, at the desired repetition rate, part of the passing signal pulse out of the optical resonator.

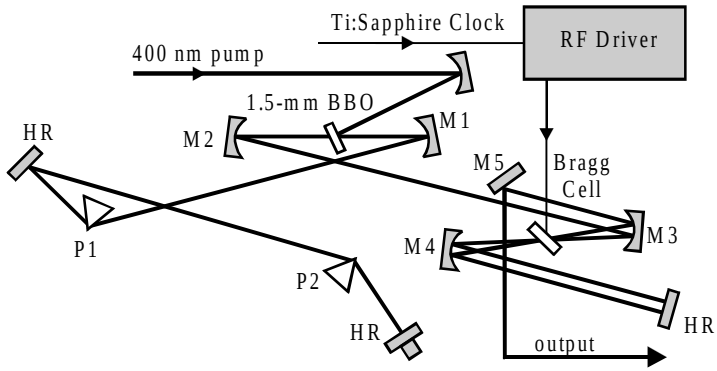

Figure 2.4. Schematics of the cavity-dumped OPO. The OPO is pumped by the second harmonic of a Ti:sapphire laser (see Fig. 2.2). M1-M4: focusing mirrors (r = -100 mm, CVI); M6: flat pick-off mirror; HR: high reflecting mirror (CVI); P1,P2: fused silica prisms; RF Driver: Spectra Physics model 454; Bragg Cell: 2-mm thick fused-silica cavity dumper (Harris). Electronic synchronization is extracted from a photodiode that tracks the repetition rate of the Ti:sapphire master oscillator. Instead of the horizontal shift indicated in the Figure, in reality the diffracted beam is vertically displaced with respect to the cavity mode.

The schematic of the cavity-dumped visible optical parametric oscillator is displayed in Figure 2.4. A linear configuration of the cavity is adopted to accommodate in its prism-less arm a Z-folded cavity-dumping unit. A 3-mm thick fused silica Bragg cell is employed that is positioned under Brewster's angle. The cavity configuration is compensated for astigmatism introduced by the Bragg cell and obeys the requirements of stability as calculated using the ABCD matrix formalism [62,65]. In the double-pass geometry of the dumper unit, the pulse traverses the acoustic-optic unit twice. When the phase of the scattered fields is properly optimized, the dumping efficiency can be significantly enhanced relative to a single pass, due to constructive interference of the scattered contributions [66,67]. Note that a similar geometry can not be incorporated in a ring cavity. Our choice of a linear cavity design was motivated by the notion that a higher dumped pulse energy is obtained with the double-pass configuration in the linear oscillator, relative to the uni-directional circular resonator.

The output coupler is substituted with a high reflective dielectric mirror to optimize the intracavity power. A fast-photodiode that monitors the mode-locking frequency of the Ti:sapphire laser delivers the triggering signal for the Bragg cell driver. A mirror

placed in the close vicinity of the dumper serves to pick off the dumped output after its second pass through the Bragg cell.

With the cavity-dumper inserted, additional reflection losses are introduced. As a result, the threshold for lasing of the OPO increases to 650 mW of pump power. Moreover, the pump depletion reduces to approximately 40%. The Bragg cell brings in additional intracavity dispersion as well. However, a moderate adjustment of the amount of prism material proves to largely compensate for the dispersion effects [68].

When the electronically induced acoustic burst is applied, a single pulse is efficiently refracted out of the cavity. Figure 2.5 shows the intracavity pulse train during dumping at 400 kHz. The contrast ratio between the dumped pulses and adjacent pulses is at least 1:100. Immediately after the dumping event, recovery of the intracavity power is initiated. At a dumping frequency of 400 kHz, 90% of the total intracavity power has recovered within 2 µs.

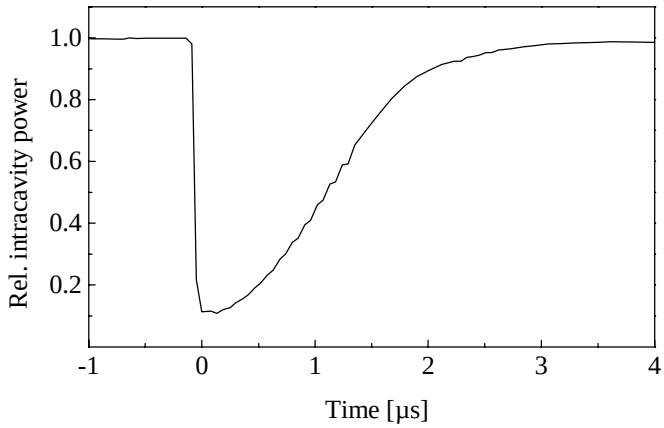

Figure 2.5. Dynamics of intracavity power after dumping with 90% efficiency at 400 kHz.

The details of transient build-up dynamics show a dependence on dumping efficiency and pulse extraction rate. Contrary to cavity-dumped Kerr-lens mode-locked laser systems, the intracavity pulse energy gradually approaches its pre-dumped level without going through an overshoot [69]. This observation reflects the different origin of the gain mechanism.

In the instantaneous parametric process, energy storage and relaxation oscillations associated with population inversion are absent. Instead, the complex build-up dynamics are governed by the spatio-temporal interaction of the pump and the circulating signal beam. In this regard it is notable that oscillation of the recovering intracavity power is obtained for certain settings of the resonator. This feature may be possibly attributed to time-varying back-conversion of signal pulse energy to the synchronized pump beam [57,58].

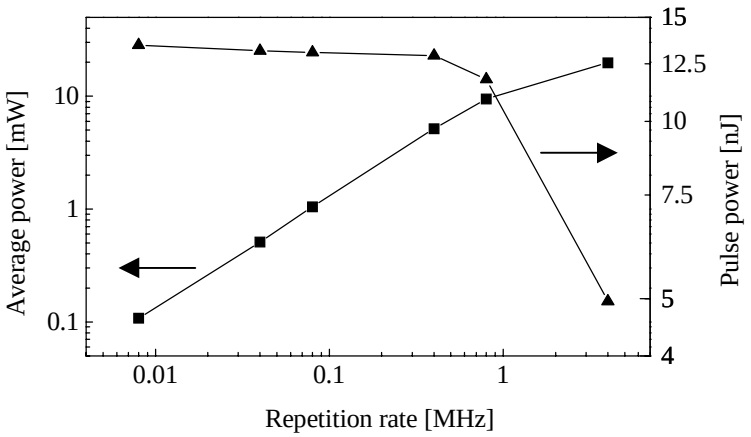

Figure 2.6. Output power of the cavity dumped OPO as a function of repetition rate. Squares represent the total average power while triangles refer to the corresponding pulse powers.

For stable operation, the typical dumping efficiency amounts to ~75% at the 400 kHz repetition rate. However, maximum efficiencies more than 90% can be obtained at lower rates. The corresponding pulse energy saturates at 13 nJ, as illustrated in Figure 2.6. The OPO functions as stable at higher dumping rates at the expense of the pulse energy. For instance, at 4 MHz the pulse energy decreases to 5 nJ as a consequence of non-complete recovery of the intracavity power between the dumping events. The stability of the cavity-dumped oscillator resembles that of the unperturbed resonator, with energy output fluctuations of less than 5%.

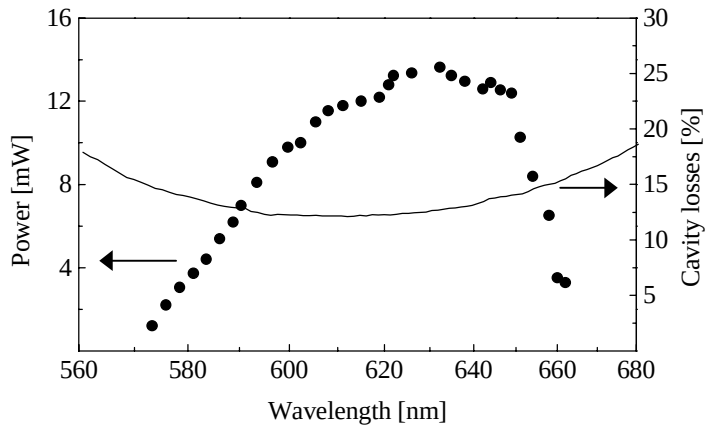

Figure 2.7. Tunability characteristics of the cavity-dumped OPO. Filled circles correspond to pulse energy as a function of the central wavelength. Solid line refers to the calculated total reflective losses for a single cavity round-trip.

The tunability curve of the cavity-dumped OPO is shown in Figure 2.7. Pulse energies of more than 12 nJ are observed between 610 nm and 650 nm. Near the tuning boundaries the dumped output power decreases as a result of intracavity reflection losses. The full tunability interval extends from 570 nm to 662 nm. Compared to the oscillator lacking the cavity-dumper optics, the tunable range is somewhat reduced. The latter observation is attributed to the perturbing action of the dumping event, which is most harmful when the OPO operates close to its threshold for lasing. In addition, the appended reflective properties of the focal mirrors and the acoustic optic element introduce optical losses, which limit stable cavity-dumping at the tuning margins. It should be noted that the spectral tunability depicted in Fig 2.7 was obtained without angular adjustment of the BBO crystal. Upon optimizing the phasematching angle close to the tuning limits, the tunability can be extended with ~10 nm at either side of the spectral range.

2.3.2 Dispersion and pulse duration

Because of the fixed roundtrip time set by the synchronously pumping, minimizing the intracavity dispersion is essential to accommodate a broad pulse spectrum in the OPO cavity. In the cavity-dumped OPO, dispersion mainly results from the presence of the BBO crystal and the Bragg cell. These elements both give rise to positive dispersion of the signal frequencies. A conventional intracavity prism compressor provides a means to counterbalance this effect. In the visible region of the spectrum, however, the negative dispersion introduced by the fused silica prism pair extends over a limited spectral range beyond which positive dispersion takes over. This feature is illustrated in Fig. 2.8a where the central signal emission wavelength is monitored as a function of cavity length. In changing the length of the cavity, only those optical wavelengths are selected whose dispersion-related roundtrip times synchronize with the repetition rate of the master oscillator. Due to the dispersive properties of the compressor two frequencies can be simultaneously generated for a fixed cavity length. As explained in Fig. 2.8b, the two branches of the tuning curve correspond to either positive or negative group delay dispersion (GDD). The slope of the profile relates to the spectral width of the pulses supported by the resonator. When tuning towards the degeneracy point, the pulse spectra become broader and eventually merge.

Broad signal spectra, which support sub-20-fs pulses, are obtained in the vicinity of the bending point where the net GDD is zero. Nonetheless, when operating in this specific region, the OPO is extremely sensitive to minute cavity length fluctuations. As a consequence, the accompanying spectral and power level oscillations prevent the OPO from stable operation.

In increasing the amount of prism material in the optical path of the resonator, the spectral position of the bending point can be shifted towards shorter wavelengths. Similarly, the point of zero net GDD is tuned to longer wavelengths when less prism material is utilized. Broad pulse spectra can thus be obtained over the entire spectral tuning range. Note that theoretically even broader spectral pulse widths can be obtained in case a less dispersive prism material like CaF_2 or MgF_2 is adopted.

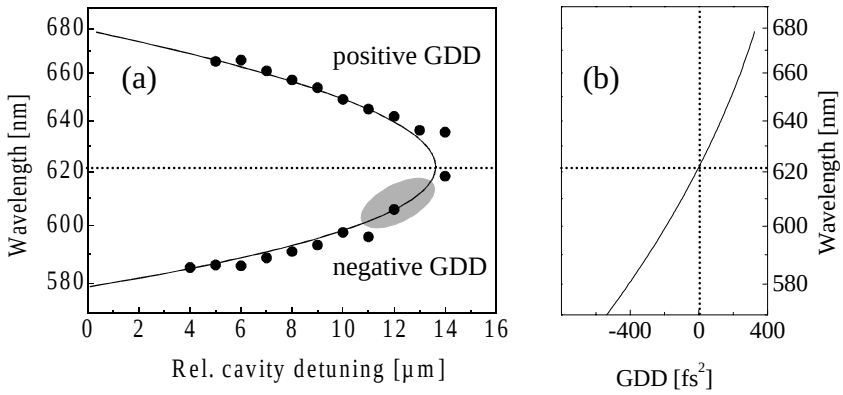

Figure 2.8. Intra-cavity dispersion characteristics. (a) Variation in the generated wavelengths for various settings of the cavity-length mismatch. Measurements were realized for a single setting of the prism pair. Filled circles mark the experimental points, the solid line results from a dispersion calculation [68]. Shaded area indicates the region where the shortest and most stable pulses are obtained. (b) Calculated intra-cavity group-delay dispersion. Wavelength of zero GDD coincides with bending point in (a).

Although the OPO operates equally well in both the positive and negative GDD regimes, the shortest and most stable pulses are obtained along the negative branch near the degeneracy point (shaded area in Fig. 2.8a). Furthermore, the addition of a slit in the dispersive arm of the cavity to suppress the spectral components at the positive GDD branch, significantly enhances the overall stability. Also, elimination of the these frequency components with positive GDD yields pulses with a less complicated spectral phase profile. Therefore, although one sacrifices a broader pulse spectrum, final temporal pulse compression is considerably facilitated.

The cavity-dumped OPO pulses are compressed using a pair of LAK8 prisms separated by 25-cm to account for residual GDD. Temporal pulse widths are determined from noncollinear autocorrelation measurements. Correlations are measured in a conventional Mach-Zehnder interferometer employing a 30-µm thick BBO crystal (Eksma) to ensure that no spectral bandwidth limitations occur [70].

Fig. 2.9 depicts the intensity autocorrelation trace of dumped 587-nm pulses at a 400 kHz repetition rate. The deconvolved pulsewidth is 30 fs assuming a Gaussian intensity profile. A small asymmetry in the pulse spectrum with a tail towards the longer wavelength is discerned. This feature relates to the intracavity dispersion, which, when tuning along the negative branch, constitutes the most favorable GDD for the red side of the pulse spectrum (Fig 2.8a). Fourier-transformation of the spectrum with a constant spectral phase yields a pulse duration of 28 fs, indicating that the actual pulses are almost bandwidth-limited. Residual broadening of the pulse is attributed to uncompensated third-order dispersion contributions that are inherently introduced when operating close to the bending point.

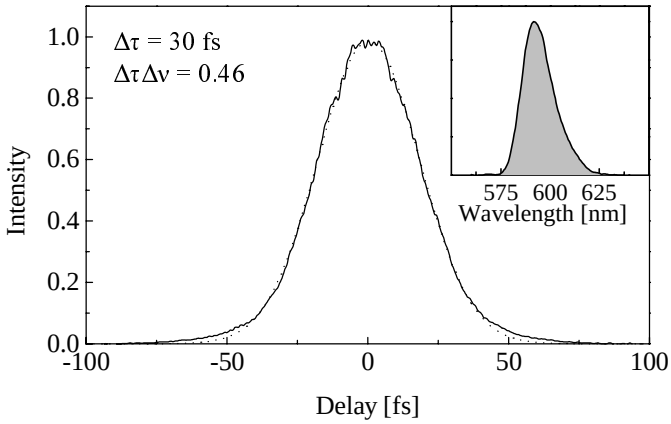

Figure 2.9. Background-free autocorrelation trace (solid line) of cavity dumped pulses at a repetition rate of 400 kHz. The dashed curve corresponds to a Gaussian fit to the data points. Inset shows the pulse spectrum.

We note that the dumped pulses are as short as the duration of pulses obtained from the oscillator without the dumper. Thus, insertion of the Bragg cell does not alter the principal features of the intracavity dispersion and retains the spectral and temporal output characteristics of the parametric oscillator.

Short pulses are obtained over the entire tuning range of the OPO as illustrated by Fig 2.10. In the central region of the tunable reach, 30-fs nearly bandwidth limited pulses are generated. Maintaining this pulse duration when tuning requires an adjustment of the prism insertion, the cavity length and the slit position simultaneously.

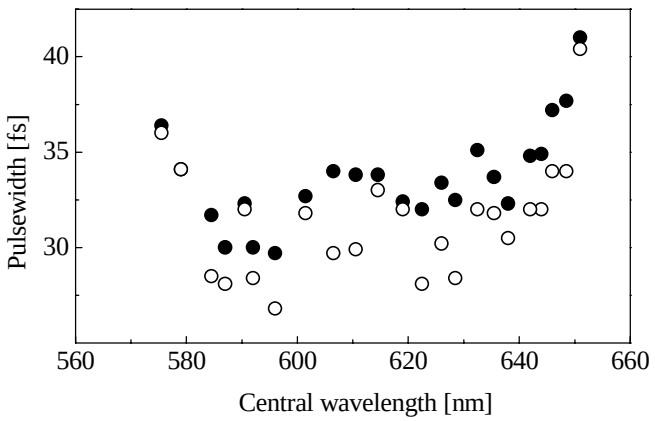

Figure 2.10. Pulse duration of dumped pulses throughout the tunable range. Pulsewidths are determined from Gaussian fits to the autocorrelation measurements (solid circles). Open circles refer to temporal widths as obtained by Fourier transforming the pulse spectra, assuming a constant phase distribution.

Near the egdes of the tuning range, the temporal widths of the pulses have somewhat broadened as a result of less efficient generation of signal frequencies towards the boundaries, thereby cutting-off of the pulse spectrum. When adjusting the repetition rate of the dumping process, the temporal pulse characteristics are not affected, implying that the cavity-dumped OPO delivers 30 fs pulses at any desirable dumping rate.

Note that longer, bandwidth limited femtosecond pulses can be easily generated when tuning away from the point of zero intracavity dispersion. In this regard, no spectral clipping is needed to narrow the pulse spectrum, thus optimizing the intracavity power. This feature is helpful in many nonlinear microscopy experiments that do not require a superb temporal resolution and are conveniently conducted with pulses of up to a few hundred femtoseconds [71].

2.4 The OPO as a multicolor light source

The cavity-dumped visible OPO system is ideally suited as an excitation light source for numerous applications in spectroscopy and optical microscopy. In particular, the tunable spectral range of the dumped pulses overlaps with the absorption spectra of an impressive series of chromophores. In addition, many natural occurring fluorophores as well as extrinsic labels can be readily excited with the visible femtosecond radiation of the OPO in a two-photon absorption process. The option of short-pulse delivery and the tunable inter-pulse interval make the system furthermore apt for accurate time-resolved spectroscopy experiments. With this source of visible radiation, many time-domain optical methods can be conducted, including fluorescence lifetime techniques, photon echo, pump-probe, transient grating and transient absorption spectroscopy [72].

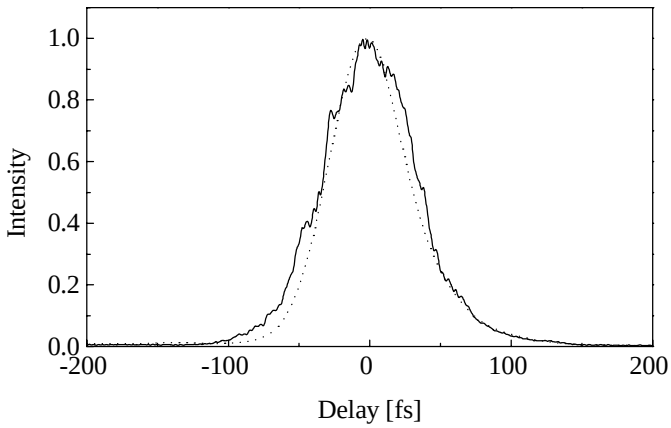

Figure 2.11. Experimental (solid line) and calculated (dashed line) crosscorrelation traces of Ti:sapphire (50-fs at 800 nm) and cavity-dumped OPO (35-fs at 630 nm). A comparison between the calculated and measured curves reveals a time-jitter of 30-fs.

Next to the tunable visible output, the Ti:sapphire-pumped OPO simultaneously provides the experimentalist with two fixed laser beams of 800 nm and 400 nm, with power levels of 850 mW and 600 mW at 82 MHz, respectively. As an intrinsic property of the synchronously pumped OPO, the repetition rates of these additional beams are directly connected to the dumping frequency of the visible radiation. Therefore, the visible OPO system constitutes a versatile light source for multicolor optical experiments such as two-color pump-probe and coherent anti-Stokes Raman scattering.

When used in nonlinear time-resolved experiments, it is crucial that the time-jitter between these pulses of the separate beams is minimized. A measure of the time-jitter is obtained by cross-correlating the output beams. Figure 2.11 shows the cross-correlation of the cavity-dumped OPO pulses with the residual beam of the Ti:sapphire laser. The correlation signal is measured using a modified Mach-Zehnder interferometer and a 30-µm BBO crystal to generate the sum-frequency signal. Individual pulse shapes required to simulate the cross-correlation, are derived from a deconvolution method based on the separately-measured autocorrelations and spectra [73,74]. As one can judge, the experimental and calculated cross-correlations match very well. The small additional broadening of the experimental trace is attributed to time-jitter that amounts to ~ 30 fs. This value is a factor of 2 smaller than the one previously reported for a KTP-based OPO [71], due to the presence of the active length stabilization. The time-jitter is considerably smaller than the Ti:sapphire pulse duration, implying that a multi-color experiment is primarily limited by pulse widths rather than by time-jitter.

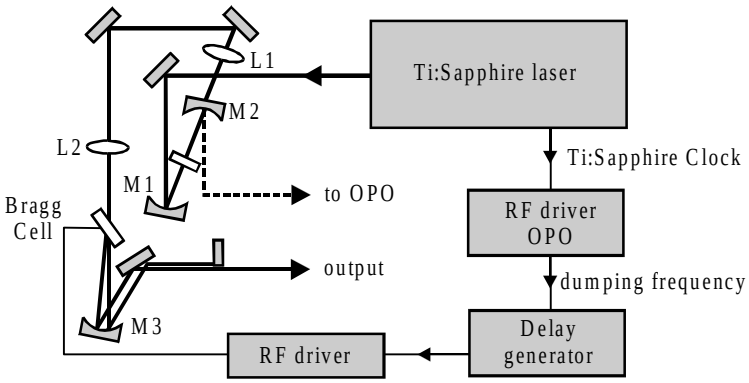

Figure 2.12. Scheme for pulse-picking of the Ti:sapphire laser output. M1,M3: focusing mirror (r = -100 mm,CVI); M2: focusing mirror (r = -125 mm,CVI), transparent for 800 nm; L1: compensating lens (f =150 mm); L2: lens (f = 200 mm); Bragg Cell: 2-mm fused silica dumper unit (Harris); RF Driver OPO: driver that controls the cavity dumper of the OPO (see Fig 2.4); RF Driver: Camac Systems model CD 5000 and PB 1800 (16 W total RF power). Delay generator: Berkeley Nucleonics Corp. model 7030. Non-diffracted beam is attenuated with an iris diaphragm.

The repetition rate of the Ti:sapphire pump beams is fixed at 82 MHz. With the OPO operating typically at sub-MHz dumping frequencies, multicolor interaction only occurs with a fraction of the Ti:sapphire pump. Hence, an unnecessary amount of the pump radiation is applied to the sample, which may invoke a thermal load or unwanted photo-induced molecular damage. This is of particular importance in the microscopic examination of live cells that are extremely susceptible to high doses of excitation light. In order to equalize the repetition rates of the pulses involved, we have utilized an acoustic-optic pulse-picker to select the pulses of the 800 nm pump beam. In Fig. 2.12 the scheme associated with the pulse selection is given. A triggering signal at the desired dumping frequency is extracted from the OPO dumper driver. The second RF driver fires when ever a trigger signal is delivered at its input. An intrinsic electronic delay of the trigger prevents one to select those pulses from the pump beam that are synchronously connected with the cavity-dumped pulses. Instead, an additional delay is deliberately introduced to pick out the very next pulse. This pulse appears after a time-interval, as set by the time in between the dumping events, has lapsed. At a dumping rate of 400 kHz, for instance, a time delay of 2.5 μs is required. The subsequent signal is amplified and used to launch an acoustic burst in a 3-mm thick Bragg cell. At 800 nm, a pulse extraction efficiency of 30% is obtained. Note that a similar scheme can be adopted to scale down the repetition rate of the 400 nm pump beam.

2.5 Conclusions

In this chapter we have discussed a versatile light source that delivers 30-fs pulses in the visible spectral regime at various repetition rates. The system employs the large parametric bandwidth of BBO under a noncollinear excitation geometry to generate tunable parametric signal between 570 and 662 nm.

The group delay dispersion in the cavity, which is largely shaped by the prism compressor, allows the generation of two colors simultaneously. Short 30 fs pulses are obtained close to the point of zero intracavity GDD. In tuning the net intracavity dispersion, the OPO produces bandwidth limited pulses up to 100 fs. This flexibility underlines the utility of the visible OPO for time-resolved experiments that require a high temporal resolution as well as for nonlinear methods, such as two-photon microscopy, in which the availability of sub-50-fs pulses is not a primary necessity.

Inserting a cavity-dumper into the oscillator significantly extends the qualification of the Ti:sapphire-pumped OPO as an excitation source for nonlinear optical microscopy. As explained in this chapter, the optical parametric oscillator can be successfully cavity-dumped without sacrificing much of the output characteristics of the resonator in terms of tunability and pulse duation. Intracavity pulse energies can be ejected from the oscillator with efficiencies of up to 90%. At 400 kHz, dumped peak powers of 13 nJ are obtained. The ability to control the repetition rate of the synchronously pumped OPO provides an additional handle to balance the moderately-high pulse energies with benign average power levels. With this excitation light, single-shot nonlinear optical signals can be readily induced in a wide variety of sample objects, including biological materials, without inflicting photodamage or heat accumulation.

Two well-synchronized pump beams at 800 nm and 400 nm are simultaneously available with the tunable radiation of the OPO. Both beams can be utilized to address

many chromophores of interest in a confocal- or two-photon optical microscope. For instance, several mutants of the green fluorescent protein can be efficiently excited with either 400 nm or via a two-photon absorption process using the 800 nm radiation [75-77]. Similarly, commonly used fluorescent labels such as DAPI and fluorescein-based markers fall within the addressable reach of these beams [78]. When used in conjunction with the visible parametric signal, various multi-color experiments can be conducted. Examples include coherent anti-Stokes Raman scattering (CARS) microscopy, which was recently shown to constitute a promising tool for the visualization of non-fluorescing probes in biological samples [4]. In addition, the limited time-jitter of only 30 fs between the OPO and the Ti:sapphire source allows the application of time-resolved experiments such as two-color pump-probe methods with a correspondingly high time-resolution.

Both the spectral and temporal properties of the BBO-based OPO, combined with the capability to vary the inter-pulse spacing with any integer number of oscillator roundtrips, make this device an almost ideal light source for (non-)linear optical microscopy [79]. Its robustness, excellent noise characteristics and multicolor beam output add furthermore to establish the OPO system as a promising excitation source for of a wide range of nonlinear optical methods among which photon-echo, transient grating and pump-probe spectroscopy [72].

Even shorter pulses may be attained when the intracavity group delay dispersion is appropriately controlled. This can for instance be accomplished when utilizing low-dispersive prism materials in combination with chirped high reflective mirrors [80,81]. Ultimate control of the cavity dispersion may eventually lead to the generation of ~5 fs pulses [82].

We finally note that the technique of cavity-dumping may also be applied to near-infrared optical parametric oscillators. Using tellerium oxide as the Bragg cell material, we anticipate that pulses from infrared devices can be dumped with a high efficiency as well.

References

1. W. Denk, J.H. Strickler and W. W. Webb, "Two-photon laser scanning fluorescence microscopy", *Science* **248**, 73-76 (1990).
2. P.J. Campagnola, M. Wei, A. Lewis and L. M. Loew, "High-resolution nonlinear optical imaging of live cells by second harmonic generation", *Biophys. J*. **77**, 3341-3349 (1999).
3. Y. Barad, H. Eisenberg, M. Horowitz and Y. Silberberg, "Nonlinear scanning laser microscopy by third harmonic generation", *Appl. Phys. Lett*. **70** 922-924 (1997); M. Müller, J. Squier, K. R. Wilson and G.J. Brakenhoff, "3D microscopy of transparent objects using third-harmonic generation", *J. Microsc*. **191,** 266-274 (1998).
4. A. Zumbusch, G.R. Holtom and X. S. Xie, "Three-dimensional vibrational imaging by coherent anti-Stokes Raman scattering", *Phys. Rev. Lett*. **82,** 4142-4145 (1999); M. Müller, J. Squier, C.A. de Lange, and G.J. Brakenhoff, "CARS microscopy with folded BoxCARS phasematching", *J. Microsc*. **197,** 150-158 (2000).
5. R. M. Williams, D. Piston and W. W. Webb, "Two-photon molecular excitation provides intrinsic 3-dimensional resolution for laser-based microscopy and microphotochemistry", *FASEB J*. **8**, 804-813 (1994).
6. W. Denk and K. Svoboda, "Photon upmanship: why multiphoton imaging is more than a gimmick", *Neuron* **18**, 351-357 (1997).
7. S. W. Hell, P. E. Hänninen, J. Salo, A. Kuusisto, E. Soini, T. Wilson and J. B. Tan, "Pulsed and cw confocal microscopy: a comparison of resolution and contrast", *Opt. Comm*. **113**, 144-152 (1994). S. Anderson-Engles, I. Rokahr and J. Carlsson, "Time- and wavelength-resolved spectroscopy in two-photon excited fluorescence microscopy", *J. Microsc*. **176**, 195-203 (1994).
8. C. Xu, W. Zipfel, J. B. Shear, R. M. Williams and W. W. Webb, "Multiphoton fluorescence: new spectral windows for biological nonlinear microscopy", *Proc. Natl. Acad. Sci. USA* **93**, 10763-10768 (1996).
9. G. J. Brakenhoff, J. Squier, T. Norris, A. C. Bliton, M. H. Wade and B. Athey, "Real-time two-photon confocal microscopy using a femtosecond, amplified Ti:sapphire system", *J. Microsc*. **181**, 252-259 (1996); W. G. Fisher, E. A. Wachter, M. Armas and C. Seaton, "Titanium:sapphire laser as an excitation source in two-photon spectroscopy", *Appl. Spec*. **51**, 218-226 (1997).
10. S. Maiti, J. B. Shear, W. R. Zipfel, R. M. Williams and W. W. Webb, "Measuring serotonin distribution in live cells with three-photon excitation", *Science* **275**, 530-532 (1997); J. B. Shear, C. Xu and W. W. Webb, "Multiphoton-excited visible emission by serotonin solutions", *Photochem. Photobiol*. **65**, 932-936 (1997).
11. B. Kierdaszuk, I. Gryczynski, A. Modrak-Wojcik, A. Bzowska, D. Shugar and J. R. Lakowicz, "Fluorescence of tyrosine and tryptophan in proteins using one-and two-photon excitation", *Photochem. photobiol*. **61**, 319-324 (1995).
12. J. A. Armstrong, N. Bloembergen, J. Ducuing and P. S. Pershan, "Interactions between light waves in a nonlinear dielectric", *Phys. Rev*. **127**, 1918-1939 (1962).
13. S. A. Akmanov and R. V. Khokhlov, "Concerning one possibility of amplification of light waves", *Sov. Phys. JETP* **16**, 252-254 (1963).
14. J. A. Giordmaine, "Mixing of light beams in crystals", *Phys. Rev. Le*t. **8**, 19-20 (1962).
15. C. C. Wang and G. W. Racette, "Measurement of parametric gain accompanying optical difference frequency generation", *Appl. Phys. Lett*. **6**, 169-171 (1965).
16. R. L. Byer, Optical parametric oscillators, Quantum Electronics, Vol. 1, Part B, edited by H. Rabin and C. L. Tang, pp 587-702 (1973).
17. K. P. Burneika, M. V. Ignatavichus, V. I. Kabelka, A. S. Piskarskas and A. Y. Stabinis, "Parametric generation of ultrashort pulses of tunable-frequency radiation", *JETP Lett*. **18**, 257-258 (1972).

18. A. Piskarskas, V. Smilgyavichyus and A. Unbrass, "Continuous parametric generation of picosecond light pulses", *Sov. J. Quant. Elect.* **18**, 155-156 (1988).
19. D. C. Edelstein, E. S. Wachman and C. L. Tang, "Broadly tunable high repetition rate femtosecond optical parametric oscillator", *Appl. Phys. Lett.* **54**, 1728-1730 (1989).
20. Q. Fu, G. Mak and H. M. van Driel, "High-power, 62-fs infrared optical parametric oscillator synchronously pumped by a 76-MHz Ti:sapphire laser", *Opt. Lett.* **17**, 1006-1008 (1992).
21. L. E. Myers, R. C. Eckardt, M. M. Fejer, R. L. Byer, W. R. Bosenberg and J. W. Pierce, "Quasi-phase-matched optical parametric oscillators in bulk periodically poled $LiNbO_3$", *J. Opt. Soc. Am. B* **12**, 2102 (1995); H. Karlsson and F. Laurell, "Electric field poling of flux grown $KTiOPO_4$", *Appl. Phys. Lett.* **71**, 3474-3476 (1997).
22. Y. Cui, M. H. Dunn, C. J. Norrie, W. Sibbett, B. D. Sinclair, Y. Tang and J. A. C. Terry, "All-solid-state optical parametric oscillator for the visible", *Opt. Lett.* **17**, 646 (1992); Y. Cui, D. E. Withers, C. F. Rae, C. J. Norrie, Y. Tang, B. D. Sinclair, W. Sibbett and M. H. Dunn, "Widely tunable all-solid-state optical parametric oscillator for the visible and near infrared", *Opt. Lett.* **18**, 122-124 (1993); P. E. Britton, D. Taverner, K. Puech, D. J. Richardson, P. G. R. Smith, G. W. Ross and D. C. Hanna, "Optical parametric oscillation in periodically poled lithium niobate driven by a diode-pumped Q-switched erbium fiber laser", *Opt. Lett.* **23**, 582-584 (1998); L. E. Myers, G. D. Miller, R. C. Eckardt, M. M. Fejer, R. L. Byer and W. R. Bosenberg, "Quasi-phase-matched 1.064-µm-pumped optical parametric oscillation in bulk periodically poled $LiNbO_3$", *Opt. Lett.* **20**, 52-54 (1995).
23. M. Ebrahimzadeh, G. P. A. Malcolm and A. I. Ferguson, "Continuous-wave mode-locked optical parametric oscillator synchronously pumped by a diode-laser-pumped solid-state laser", *Opt. Lett.* **17**, 183-185 (1992); M. J. McCarthy and D. C. Hanna, "Continuous-wave mode-locked singly resonant optical parametric oscillator synchronously pumped by a laser-diode-pumped Nd:YLF laser", *Opt. Lett.* **17**, 402 (1992).
24. G. Szabó and Z. Bor, "Frequency conversion of ultrashort pulses", *Appl. Phys. B* **58**, 237-241 (1994).
25. R. Danielius, A. Piskarskas, P. Di Trapani, A. Andreoni, C. Solcia and P. Foggi, "Matching of group velocities by spatial walk-off in collinear three-wave interaction with tilted pulses", Opt. Lett. **21**, 973-975 (1996).
26. R. L. Byer and A. Piskarskas; eds., feature on optical parametric oscillators and amplification, *J. Opt. Soc. Am. B* **30**, 1656-2243 (1993).
27. R. Beigang, ed., feature on cw mode-locked optical parametric oscillators, *Appl. Phys. B* **60**, 409-467 (1995).
28. W. R. Bosenberg and R. C. Eckhardt, feature on optical parametric devices, *J. Opt. Soc. Am. B* **12**, 2087-2322 (1995).
29. M. Ebrahimzadeh, R. C. Eckardt and M. H. Dunn, feature on optical parametric devices and processes, *J. Opt. Soc. Am. B* **16**, 1477-1597 (1999).
30. M. H. Dunn and M. Ebrahimzadeh, "Parametric generation of tunable light from continuous-wave to femtosecond pulses", *Science* **286**, 1513-1517 (1999).
31. P. J. Phillips, S. Das and M. Ebrahimzadeh, "High-repetition-rate, all-solid-state, Ti:sapphire-pumped optical parametric oscillator in the mid-infrared", *Appl. Phys. Lett.* **77**, 469-471 (2000); K. L. Vodopyanov, F. Ganikhanov, J. P. Maffetine I. Zwieback and W. ruderman, "ZnGeP2 optical parametric oscillator with 3.8-12.4 µm tunability", *Opt. Lett.* **25**, 841-843 (2000).
32. S. Meyer, B. N. Chichkov and B. Wellegehausen, "High-order parametric amplifiers", *J. Opt. Soc. Am. B* **16**, 1587-1591 (1999).
33. T. S. Sosnowski, P. B. Stephens and T. B. Norris, "Production of 30-fs pulses tunable troughout the visible specral region by a new technique in optical parametric amplification", *Opt. Lett.* **21**, 140-142 (1996).

34. G. Schweitzer, L. Xu, B. Craig and F. C. De Schryver, "A double OPA femtosceond laser system for transient absorption spectroscopy", *Opt. Comm.* **142**, 283-288 (1997).
35. A. Shirakawa and T. Kobayashi, "Noncollinear phase-matched femtosecond optical parametric amplification with a 2000 cm^{-1} bandwidth", *Appl. Phys. Lett*. **72**, 147-149 (1998); A. Shirakawa, I. Sakane and T. Kobayashi, "Pulse-front-matched optical parametric amplification for sub-10-fs pulse generation tunable in the visble and near infrared", *Opt. Lett*. **23**, 1292-1294 (1998).
36. K. S. Wong, Z. R. Qui, H. wang and G. K. L. Wong, "Efficient visible femtosecond optical parametric generator and amplifier using tilted pulse-front pumping", *Opt. Lett*. **22**, 898-900 (1997).
37. A. L. Oien, I. T. McKinnie, P. Jain, N. A. Russell, D. M. Warrington and L. A. W. Gloster, "Efficient low-treshold collinear and noncollinear β-barium borate optical parametric oscillators", *Opt. Lett*. **22**, 859-861 (1997).
38. T. Wilhelm, J. Piel and E. Riedle, "Sub-20-fs pulses tunable across the visible from a blue-pumped single-pass noncollinear parametric converter", *Opt. Lett*. 22, 1494-1496 (1997).
39. G. Cerullo, M. Nisoli and S. Di Silvestri, "Generation of 11 fs pulses tunable across the visible by optical parametric amplification", Appl. Phys. Lett. **71**, 3616-3618 (1997).
40. G. Cerullo, M. Nisoli, S. Stagira and S. De Silvestri, "Sub-8-fs pulses from an ultrabroadband optical parametric amplifier in the visible", *Opt. Lett*. 16, 1283-1285 (1998).
41. R. J. Ellington and C. L Tang, "High-power, high-repetition-rate femtosecond pulses tunable in the visible", *Opt. Lett*. **18**, 438-440 (1993); A. Shirakawa, H. W. Mao and T. Kobayashi, "Highly efficient generation of blue-orange femtosecond pulses from intracavity-frequency-mixed optical parametric oscillator", *Opt. Comm.* **123**, 121-128 (1996).
42. A. Nebel, H. Frost, R. Beigang and R. Wallenstein, "Visible femtosecond pulses by second-harmonic generation of a cw mode-locked KTP optical parametric oscillator", *Appl. Phys. B* **60**, 453-458 (1995);
43. S. French, M. Ebrahimzadeh and A. Miller, "High-power, high-repetition-rate picosecond optical parametric oscillator tunable in the visible", *Opt. Lett*. **21**, 976-978 (1996).
44. T. J. Driscoll, G. M. Gale and F. Hache, "Ti:sapphire second-harmonic-pumped visible range femtosecond optical parametric oscillator", *Opt. Comm*. **110**, 638-644 (1994).
45. G. M. Gale, M. Cavallari, T. J. Driscoll and F. Hache, "Sub-20 fs tunable pulses in the visible from an 82-MHz optical parametric oscillator", *Opt. Lett*. **20**, 1562-1564 (1995).
46. E. P. Buurman, R. Sanders, A. Draaijer, H. C. Gerritsen, J. J. F. van Veen, P. M. Houpt and Y. K. Levine, "Fluorescence lifetime imaging using a confocal laser scanning microscope", *Scanning* **14**, 155-159 (1992); J. Sytsma, J. M. Vroom, C. J. de Grauw and H. C. Gerritsen, "Time-gated fluorescence lifetime imaging and microvolume spectroscopy using two-photon excitation", *J. Microsc*. **191**, 39-51 (1998).
47. A. Cybo-Ottone, M. Nisoli, V. Magni, S. De Silvestri and O. Svelto, "Highly stable 60 fs pulses form a cavity dumped hybridly mode-locked day laser", Opt. Comm. **92**, 271-276 (1992).
48. M. Ramaswamy, M. Ulman, J. Paye and J. G. Fuijmoto, "Cavity-dumped femtosecond Kerr-lens mode-locked Ti:Al_2O_3 laser", *Opt. Lett*. **18**, 1822-1824 (1993).
49. M. S. Psenichnikov, W. P. de Boeij and D. A Wiersma, "Generation of 13-fs, 5-MW pulses from a cavity-dumped Ti:sapphire laser", *Opt. Lett*. **19**, 572-574 (1994).
50. E. Slobodchikov, J. Ma, V. Kamlaov, K. Tominaga and K. Yoshihara, "Cavity-dumped femtosecond Kerr-lens mode locking in a chromium doped fosterite laser", *Opt. Lett*. **21**, 354-356 (1996).
51. G. N. Gibson, R. Klank, F. Gibson and B. E. Bouma, "Electro-optically cavity-dumped ultrashort-pulse Ti:sapphire oscillator", *Opt. Lett*. **21**, 1055-1057 (1996).

52. E. O. Potma, W. P. de Boeij. M. S. Psenichnikov and D. A. Wiersma, "A 30-fs, cavity-dumped optical parametric oscillator", *Opt. Lett.* **23**, 1763-1765 (1998).
53. V. G. Dmitriev, G. G. Gurzadyan and D. N. Nikogosyan, Handbook of nonlinear optical crystals, Springer Verlag Heidelberg, 1999, chapter 2.
54. T. Nishikawa and N. Uesugi, "Walk-off and pump energy dependence of transverse beam profiles on travelling wave parametric generation", *Opt. Comm* **140**, 277-280 (1997).
55. H. J. Bakker, P. C. M. Plancken and H. G. Muller, "Numerical calculation of frequency-conversion processes: a new approach", *J. Opt. Soc. Am B* **6**, 1665-1672 (1989); E. C. Cheung and J. M. Liu, "Theory of synchronously pumped optical parametric oscillaor in steady-state operation", *J. Opt. Soc. Am. B* **7**, 1385-1401 (1990).
56. A. Hasché, G. R. Allen and H. M. van Driel, "Effects of cavity detuning on the pulse characteristics of a femtosecond synchronously pumped optical parametric oscillator", *J. Opt. Soc. Am. B* **12**, 2209-2213 (1995).
57. G. M. Gale, M. Cavallari and F. Hache, "Femtosecond visible optical parametric oscillator", *J. Opt. Soc. Am. B* **15**, 702-714 (1998).
58. F. Hache, A. Zéboulon, G.Gallot and G. M. Gale, "Cascaded second-order effects in the femtosecond regime in β-barium borate: self-copression in a visible femtosecond optical parametric oscillator", *Opt. Lett*. **20**, 1556-1558 (1995).
59. D. Eimerl, L. Davis, S. Velsko, E. K. Graham and A. Zalkin, "Optical, mechanical, and thermal properties of barium borate", *J. Appl. Phys*. **62**, 1968-1983 (1987).
60. P. Di Trapani, A. Andreoni, G. P. Banfi, C. Solcia, R. Danielus, A. Piskarskas, P. Foggi, M. Monguzzi and C. Sozzi, "Group-velocity self-matching of femtosecond pulses in noncollinear parametric generation", *Phys. Rev. A*. **51**, 3164-3168 (1995); P. Di Trapani, A. Andreoni, C. Solcia, P. Foggi, R. Danielius, A. Dubietis and A. Piskarskas, "Matching of group velocities in three-wave parametric interaction with femtosecond pulses and application to traveling-wave generators", *J. Opt. Soc. Am B* **12**, 2237-2244 (1995).
61. R. Urschel, U. Bäder, A. Borsutzky and R. Wallenstein, "Spectral properties and conversion efficiency of 355-nm-pumped pulsed optical parametric oscillators of b-barium-borate with noncollinear phase-matching", *J. Opt. Soc. Am B* **16**, 565-579 (1999).
62. A. E. Siegman, "Lasers", University Science, Mill Valey, California (1986).
63. D. E. Spence, W. E. Sleat, J. M. Evans, W. Sibbet and J.D. Kafka, "Time synchronization measurements between two self-modelocked Ti:sapphire lasers", *Opt. Comm*. **101**, 286 (1993).
64. J. Chesnoy and L. Fini, "Stabilization of a femtosecond dye laser synchronously pumped by a frequency-doubled mode-locked YAG laser", *Opt. Lett*. **11**, 635-637 (1986).
65. H. W. Kogelnik, E. P. Ippen, A. Dienes, C. V. Shank, "Atigmatically compensated cavities for CW dye lasers", *IEEE J. Quantum. Electron*. **8**, 373 (1972).
66. Spectra-physics, instruction manual, Model 344S cavity dumper & Model 454 cavity dumper driver.
67. W. P. de Boeij, "Ultrafast Solvation Dynamics Explored by Nonlinear Optical Spectroscopy", *thesis*, University of Groningen, 1997.
68. Calculations were performed to quantitate the intra-cavity dispersion. The ray-tracing computations take into the consideration the refractive indices of the optical components and the settings of the intra-cavity prism compressor.
69. G. M. Gibson, G. R. Morrison, P. L Hansen, M. H. Dunn and M. J. Padgett, "Dynamic behaviour of a doubly resonant optical parametric oscillator", *Opt. Comm*. **136**, 423-428 (1997).
70. A. M. Weiner, "Effect of group velocity mismatch on the measurement of ultrashort optical pulses via second harmonic generation", *IEEE J. Quantum. Electron*. **19**, 1276-1283 (1983).

71. K. König, T. W. Becker, P. Fischer, I. Riemann and K. J. Halbhuber, "Pulse-length dependence of cellular response to intense near-infrared laser pulses in multiphoton microsopes", *Opt. Lett*. **24**, 113-115 (1999).
72. M.D. Levenson, S.S. Kano, Introduction to Nonlinear Laser Spectroscopy, Academic Press, San Diego, (1987).
73. A. Baltuška, Z. Wei, M. S. Pshenichnikov, D. A. Wiersma and R. Scipőcs, "All-solid-state cavity-dumped sub-5-fs laser", *Appl. Phys. B* **65**, 175-188 (1997).
74. J. Peatross and A. Rundquist, "Temporal decorrelation of short laser pulses", *J. Opt. Soc. Am. B* **15**, 216-222 (1998).
75. K. D. Niswender, S. M. Blackman, L. Rohde, M. A. Magnuson and D. W. Piston, "Quantitative imaging of green fluorescent protein in cultured cells: comparison of microscopic techniques, use in fusion proteins and detection limits", *J. Microsc*. **180**, 109-116 (1995).
76. R. H. Kohler, W. R. Zipfel, W. W. Webb and M. R. Hanson, "The green fluorescent protein as a marker to visualize plant mitochondria in vivo", *Plant. J*. **11**, 613-621 (1997).
77. A. Volkmer, V. Subramaniam, D. J. S. Birch and T. M. Jovin, "One- and two-photon excited fluorescence lifetimes and anisotropy of green fluorescent proteins", *Biophys. J*. **78**, 1589-1598 (2000).
78. See for an impressive list of biologically relevant fluorescent labels: Handbook of fluorescent probes and research chemicals, R. P. Haughland, Molecular Probes (1999).
79. E. O. Potma, N. Kahya, W. P. de Boeij and D. A. Wiersma, "A multicolor femtosecond light source for (multiphoton) confocal fluorescence microscopy", in: Microscopy and Microanalysis 1999, Vol. 5, suppl. 2, pages 472 – 473, edited by G.W. Baily, W. G. Jerome, S. McKernan, J. F Mansfield and R. L Price, Springer verlag (1999).
80. R. Scipőcs, K. Ferencz, C. Spielman and F. Krauz, "Chirped multilayer coatings for broadband dispersion control in femtosecond lasers", *Opt. Lett*. **19**, 201-203 (1994).
81. J. Hebling, H. Giessen, S. Linden and J. Kuhl, "Mirror-dispersion-compensated femtosecond optical parametric oscillator", *Opt. Comm*. **141**, 229-236 (1997).
82. The minimum pulse duration is calculated by Fourier transforming the field associated with the parametric spectral bandwidth as depicted in Fig. 2.1.